The Silicon Diode Array Camera Tube

By MERTON H. CROWELL and EDWARD F. LABUDA

(Manuscript received November 26, 1968)

A new electronic camera tube has been developed for Picturephone® *visual telephone applications; with minor modifications it should also be suitable for conventional television systems. The image sensing target of the new camera consists of a planar array of reversed biased silicon photodiodes which are accessed by a low energy scanning electron beam similar to that used in a conventional vidicon. This paper presents a description of the operating principles and an analysis of the sensitivity and resolution capabilities of the new silicon diode array camera tube.*

We also give the detailed experimental results obtained with the tubes. The gamma of a silicon diode array camera tube is unity and its spectral response is virtually uniform over the wavelength range from 0.45 *to* 0.90 *micron with an effective quantum yield greater than* 50 *percent. For a* 13.4 *millimeter square target the silicon diode array camera tube's sensitivity is* 20 *μamp foot-candles of faceplate illumination with normal incandescent illumination or* 1.3 *μamp per foot-candle with fluorescent illumination; with a center-to-center diode spacing of* 15 *micron it's modulation transfer function is greater than* 60 *percent for a spatial frequency of* 14 *cycles per millimeter. Typical dark currents for a* 13.4 *millimeter square target are in the range of* 5 *to* 50 *nanoamperes.*

I. INTRODUCTION

A large number of electronic cameras have been developed for converting an optical image into an electrical signal.[1-3] In many of these, a light-induced charge pattern is stored on a suitable image sensing target and a low velocity scanning electron beam is used to access the charge pattern. One such camera tube, the vidicon, has many desirable characteristics; it has found extensive commercial use partly because of small size and inexpensive construction.[2] However, the vidicon does possess characteristics which, in many applications, can prove undesirable or even detrimental.

Recently there have been several reports of development aimed at obtaining an all solid-state image-sensing system.[4–8] Typically, these systems consist of an array of photosensitive elements scanned by solid-state logic circuits. In general, the technology associated with producing the logic circuits that must duplicate the function of the scanning electron beam is quite complicated. As a result, in all such systems reported to date, the density of photosensitive elements has been rather limited, and the resulting resolution has been small compared with what can be achieved with a vidicon and what would be required in a great many applications of interest.

This paper describes a new camera tube which has the resolution, small size, and inexpensive construction of the vidicon, but not many of its undesirable features. While the vidicon has an evaporated photoconducting film as the image sensing target, the new camera has a planar array of reverse biased silicon photodiodes.[9–12] The diode side of the array is scanned by a low velocity electron beam, and the electron optics are similar to that of a conventional vidicon. Notable improvements in device performance result from the chemical stability of the planar array of silicon photodiodes. This stability insures that the target performance will not be impaired by a high temperature vacuum bake (400°C), necessary for long tube life, or by accidental exposure to intense light images or prolonged exposure to fixed images of normal intensity.

The new silicon diode array camera (SIDAC) tube has three valuable attributes:

(*i*) The spectral response is approximately constant from 0.45μ to approximately 0.90μ with an effective quantum yield of greater than 50 percent.

(*ii*) Electronic zoom can be achieved by varying the size of the raster on the mosiac of diodes since, as discussed in Section 6.2, under the proper operating conditions the scanning beam does not alter the uniformity of the target response.

(*iii*) There is no undesirable image persistance resulting from photoconductive lag.

The first two are unique to the silicon diode array camera tube; the last one is true for the Plumbicon and at high levels of illumination for the vidicon.[3]

Section II discusses the operating principles of the silicon diode array camera tube and Section III analyses its sensitivity and resolu-

tion capabilities. The results of the analysis are compared with experiments. The experimental results which are in agreement with the theoretical calculations demonstrate the feasibility of using the tube in systems requiring the quality of entertainment type television. Several alternative modifications of the basic diode array structure that are intended to improve various aspects of its performance are described in Section IV. One of these embodiments, the resistive sea structure, is discussed and analyzed in more detail in Section V. Various other miscellaneous topics, including image lag and dark current are discussed in Section VI.

Details about the target concerning fabrication techniques, X-ray imaging, and other electron imaging applications are described elsewhere.[13,14,15]

II. OPERATING PRINCIPLES OF THE DIODE ARRAY CAMERA TUBE

Figure 1 illustrates the silicon diode array camera tube. The optical image is focused by a lens onto the substrate of the photodiode array. The diode side of the array is scanned by an electron beam that has passed through the appropriate electron optics for focusing and deflection. Deflection is achieved magnetically; focus is achieved either electrostatically or magnetically. In all the experiments to be reported, the interlaced raster scanning period was 1/30 second.

Most of the experimental results given in this paper were obtained

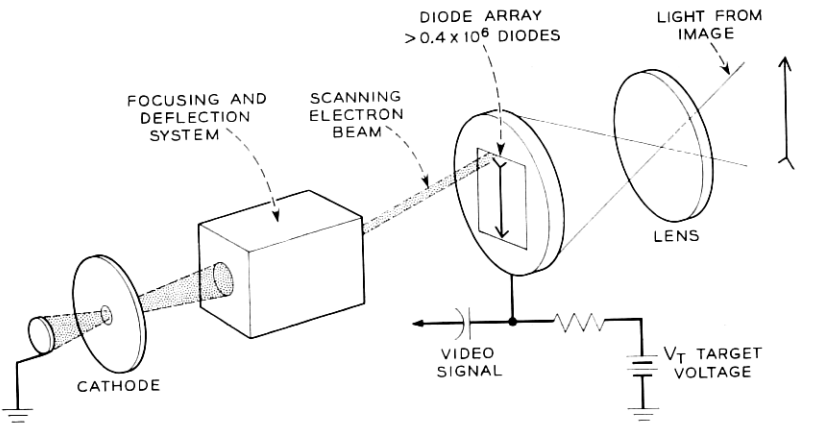

Fig. 1 — Schematic of a diode array camera tube. The electron beam scans the diode side of the array, and the optical image is focused onto the substrate of the array.

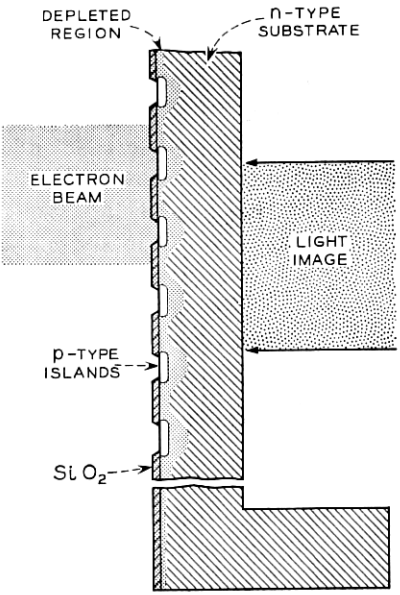

Fig. 2 — Schematic of a diode array target. To obtain a self-supporting structure, the perimeter of the wafer is left much thicker than the substrate in the area of the diode array.

with the target geometry illustrated in Fig. 2. These arrays typically consisted of a matrix of 660 by 660 diodes—about 436,000 diodes within a 0.528-inch square. The substrate is nominally 10 Ω-cm, n-type silicon with a diameter of 0.85 inch. The substrate in the area of the diode array is uniformly thick—0.2 to 2.0 mils (5–50μ)—while the perimeter of the wafer is thicker—4 mils—to ensure a self-supporting structure. The diodes, consisting of p-type islands in the n-type substrate, are formed by standard photolithographic and planar processing techniques.[13] The 660 by 660 array has a center-to-center diode spacing of 20μ and an oxide hole diameter of 8μ. In the early models gold was evaporated over a separately diffused n^+ region to ensure good electrical contact to the substrate. Subsequent experimental results have indicated that a satisfactory contact can be obtained without the evaporated gold.

In normal operation the substrate of the diode array is biased positively with respect to the cathode of the electron gun. The substrate potential relative to cathode potential is called the target voltage and is typically 10 volts. The impinging electron beam thus strikes the

mosaic with a maximum energy of 10 electron volts and deposits electrons on both the p-type islands and the silicon dioxide film surrounding the diodes, which isolates the substrate from the beam. Since the resistivity of the silicon dioxide film is very high, the electronic charge accumulates on this surface and charges it to some voltage very close to cathode potential where it remains.

The beam diameter, as indicated in Fig. 2, is generally larger than the diode spacing to eliminate any need for registration between the beam and the mosaic. The electronic charge deposited by a sufficiently intense beam will place a reverse bias of 10 volts on the diodes as it scans over the array. This bias will create a depletion width of approximately 5μ with a 10 Ω-cm substrate giving a junction capacitance that results in an effective charge storage capacitance for the target of approximately 2,000 pF per cm^2. Notice that, at this bias, the silicon surface under the oxide will normally be depleted as indicated in Fig. 2. With very low values of diode leakage currents (less than 10^{-13} amperes per diode) the diodes remain in the full reverse biased condition throughout the entire frame period, if they are not illuminated. The usable values of target capacitance are limited to a narrow range by several factors.[3] For example, the minimum useful target capacitance is determined from the ratio of the required peak video current to the permissible swing in voltage on the scanned side of the array. The maximum voltage swing of the scanned surface is limited by the allowable amount of beam bending which results from transverse (that is, parallel to the surface) electric fields. On the other hand, the maximum capacitance is limited by the charging ability of the electron beam and the image lag requirements placed on the camera. The charging ability of the beam is substantially greater for a higher positive surface potential which is inversely proportional to the target capacitance. In addition, in the diode array camera tube the maximum amount of charge that can be stored is limited by the breakdown voltage of the diodes.[12]

Almost all of the incident light associated with the image is absorbed in the n-type region, each absorbed photon giving rise to one hole-electron pair. Since the absorption coefficient for visible light in silicon is greater than 3000 cm^{-1}, the majority of the photon-generated carriers will be created near the illuminated surface.[16] This will increase the minority carrier (that is, hole) density above its thermal equilibrium value and cause a net diffusion of holes toward the reverse biased diodes. If the lifetime of the holes is sufficiently long and the illuminated surface has been treated properly to reduce

recombination effects, a large fraction of the photon-generated holes will diffuse to the electric fields associated with the depletion regions of the diodes and will contribute to the junction current. The light-induced junction current will continue to flow and discharge the junction capacitance throughout the frame period as long as the diodes remain in the reverse-biased condition. Thus, high light levels require high values of reverse-bias voltage or high values of junction capacitance to avoid saturation. The video output signal from each diode is created when the electron beam returns to a diode and restores the original charge by re-establishing the full value of reverse bias. The sensitivity and resolution capabilities of the basic diode array structure are considered in Section III.

It has been found experimentally that the basic diode array structure indicated in Fig. 2 has one rather undesirable characteristic: the silicon dioxide film which insulates the substrate from the electron beam can exhibit uncontrollable charging effects. In some cases the film will accumulate enough negative charge to repell the electron beam and prevent it from impinging on the p-regions. Several alternative modifications of the basic target structure which prevent this charging phenomenon and which improve the performance of the array in other respects are discussed in Section IV.

III. SENSITIVITY AND RESOLUTION CAPABILITIES OF A DIODE ARRAY TARGET

As described in Section II the light associated with the optical image is absorbed in the n-type substrate of the diode array creating hole-electron pairs. The photo-generated holes then diffuse from their point of generation to the depletion regions of the reverse-biased diodes. This section considers the sensitivity and resolution capabilities of the diode array target as determined by hole diffusion and the discrete nature of the diode array, but it does not consider any limitations in resolution resulting from the finite size of the electron beam, aberrations in the light optics, or frequency response of the video amplifiers.

3.1 *Diffusion of Minority Carriers*

An analytical evaluation of the diffusion process in a mosaic target would be quite complicated. In fact, an exact solution would require detailed knowledge of the shape of the depletion regions. However, to estimate the light sensitivity and resolving ability from the simplified model in Fig. 3 is quite straightforward. In this figure,

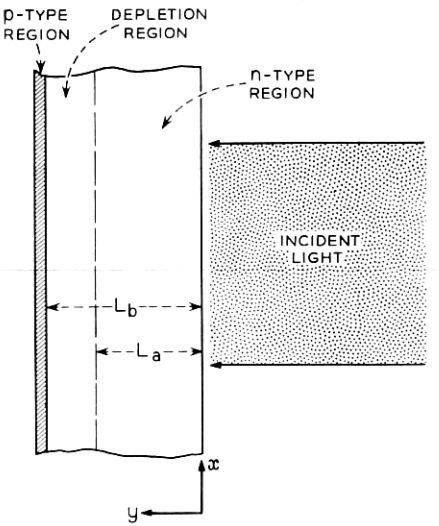

Fig. 3 — Schematic of the simplified model used to estimate the light sensitivity and resolving ability of a diode array target.

the isolated p-regions have been replaced by one homogeneous p-region in which there is no lateral conductivity. This is equivalent to a mosaic structure with zero spacing between diodes. With the low surface recombination velocity normally achieved at the silicon dioxide-silicon interface between diodes or with a fully depleted surface as shown in Fig. 2, the theoretical results obtained from the simplified model should accurately predict the sensitivity of the silicon diode array camera tube. Since the response of the tube is proportional to the incident light level (that is, the gamma is unity) camera sensitivity may be determined by calculating the ratio of the flux of optically generated holes entering the p-region to the incident photon flux.

The steady state diffusion of optically excited holes in the substrate from their point of generation to the depletion regions of the diodes will be governed by the time independent continuity equation[17]

$$-D\nabla^2 p + p/\tau = G(x, y, z) \tag{1}$$

where

p = hole density in excess of thermal equilibrium
τ = minority carrier lifetime

D = hole diffusion constant in n-type silicon
G = hole generation rate per unit volume.

For the model of Fig. 3, the appropriate boundary conditions are

$$\begin{aligned} Sp &= D\frac{\partial p}{\partial y} \qquad \text{at} \quad y = 0 \\ p &= 0 \qquad\qquad\quad \text{at} \quad y = L_a \end{aligned} \tag{2}$$

where S is the surface recombination velocity for holes at the illuminated surface. Setting $p = 0$ at $L = L_a$, the edge of the depletion region, is valid since the electric field prevents any accumulation of holes by quickly sweeping the holes across the depletion region.

The problem being considered here is similar to the one analyzed by Buck and others;[13] however, it does differ in two significant respects. First, our calculation takes into account carrier generation in the depletion regions of the diodes whereas Buck's analysis, intended for short circuit current measurements, does not include carrier generation in the junction space charge region. Second, the hole generation rate is permitted to vary in the transverse direction (the x direction of Fig. 3) so that nonuniform incident light intensities can be considered. This permits evaluation of the loss in resolution caused by lateral diffusion of the holes.

If it is assumed that the light incident on the target is stationary, monochromatic, parallel, and varying in intensity only in the transverse direction as

$$(N_0/2)(1 + \cos kx),$$

then the generation function $G(x, y, z)$ will be given by

$$G(x, y) = \frac{N_0}{2}\alpha(1 - R)(1 + \cos kx)e^{-\alpha y} \tag{3}$$

in which

N_o = peak incident photon flux,
α = silicon absorption coefficient at the optical wavelength of interest,
R = silicon reflectivity at the optical wavelength of interest,
k = 2π/[spatial period of the intensity variation in the transverse direction].

This equation does not include the response to infrared light that may be multiple reflected when the absorption coefficient becomes very

small (that is, $\alpha L_b < 2$ corresponding to optical wavelengths greater than approximately 0.8μ). With the above generation function, equation (1) can be solved, subject to the boundary conditions given in equation (2), for the hole distribution in the substrate. The hole flux entering the p-region, $J_p(x)$, can then be obtained by evaluating the hole diffusion current density that enters the depletion region and adding to this the number of holes per unit time and area created by photons absorbed in the depletion region. The result may be written in the form

$$J_p(x) = (N_0/2)\{\eta_0 + \eta_k \cos kx\} \tag{4}$$

with

$$\eta_k = \frac{\alpha L(1-R)}{\alpha^2 L^2 - 1}\left[\frac{2(\alpha L + SL/D) - (\beta_+ - \beta_-)\exp(-\alpha L_a)}{\beta_+ + \beta_-} - (\alpha L)^{-1}\exp(-\alpha L_a)\right] - (1-R)\exp(-\alpha L_b), \tag{5}$$

$$\eta_0 = \eta_k \mid_{k=0}$$

and in which

$$\begin{aligned}
\beta_\pm &= (1 \pm SL/D)\exp \pm (L_a/L),\\
1/L^2(k) &= 1/L_0^2 + k^2,\\
L_o &= \text{diffusion length} = (D\tau)^{\frac{1}{2}},\\
L_a &= \text{thickness of undepleted region},\\
L_b &= \text{thickness of the } n\text{-type region plus the width of the depletion region.}
\end{aligned}$$

Notice that η_0 is the ratio of the flux of optically generated holes entering the p-region to the incident photon flux for uniform illumination ($k = 0$).

The existence of a "dead layer" and an electric field associated with the illuminated surface, as discussed by Buck and others, invalidates the field-free continuity equation in a small region near the illuminated surface.[13] Consequently, at the shorter wavelengths ($< 0.5\mu$), measured sensitivities may be less than that predicted by equation (5).

With the above reservation in mind, η_0 versus optical wavelength for various values of the target parameters can be obtained from equation (5). For the results to be presented, the thickness of the undepleted portion of the substrate L_a was assumed to be 15μ. As Section 3.1 shows, this is a practical value since the maximum value of

L_a for an operating camera tube will be determined by the resolution requirements. The width of the depletion region was assumed to be 5μ which is appropriate for a 10 Ω-cm substrate with a target bias of approximately 10 volts. The wavelength dependence of α, the absorption coefficient, was obtained from the data of Dash and Neumann while the measured wavelength dependence of R, the reflectivity as given by the solid curve in Fig. 4, was used.[16]

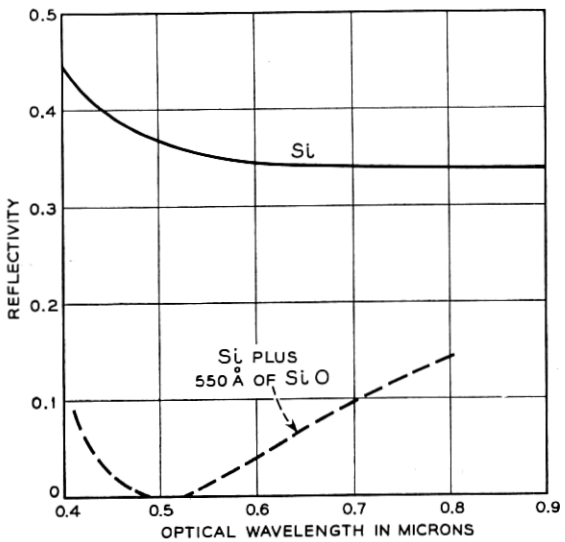

Fig. 4 — Reflectivity versus optical wavelength of a bare, polished silicon surface and of a polished silicon surface with an evaporated layer of silicon monoxide. In both cases the silicon was n-type with a resistivity of approximately 10 Ω-cm.

In Figs. 5 and 6, η_o is plotted versus wavelength for various values of L_o/L_a (or equivalently lifetime τ) for two values of S.* As expected, the curves of Fig. 6, corresponding to a surface with a relatively low recombination velocity, are much higher at the shorter wavelengths than those of Fig. 5 which correspond to a surface with a high recombination velocity. Also as expected, η_o becomes independent of τ for $L_o > L_a$.

An inspection of equation (5) in the wavelength range where $\alpha L_a \gg 1$

* The apparent discontinuity in the curves near 0.5μ results from a discontinuity in the dependence of absorption coefficient upon optical wavelength as reported in the literature and is probably spurious.

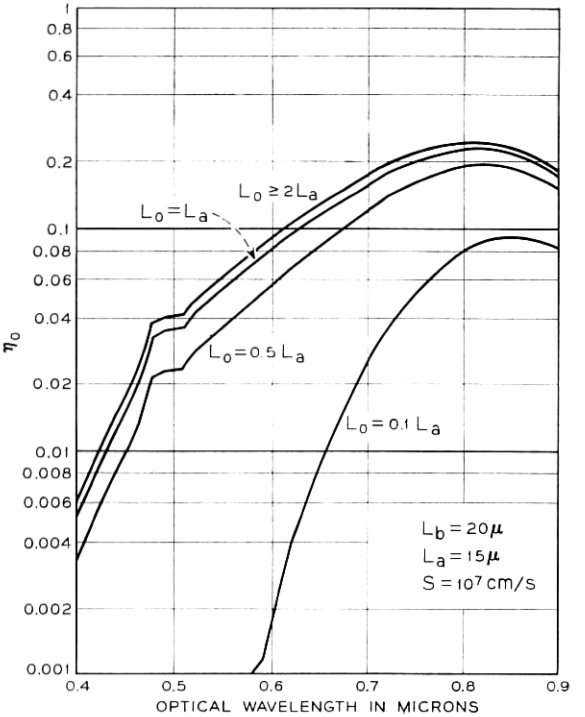

Fig. 5 — Calculated plots of η_0 versus optical wavelength for different values of minority carrier lifetime or equivalently different values of the diffusion length L_a and for a high value of surface recombination velocity S.

indicates that η_0 will be virtually independent of wavelength, except for the slight wavelength dependence of the reflectivity, if $S/D < \alpha$. This is illustrated by the curves of Fig. 7 which give η_0 versus wavelength for various values of S and a given value of τ or equivalently L_a. At the shorter wavelengths (increasing α) the curves are essentially independent of wavelength for values of S less than 10^3cm per second.

Measured values of η_0 for three diode array camera tubes with different targets are shown in Fig. 8. These results are in qualitative agreement with the above considerations. The arrays with a low recombination velocity which provide the best response for short wavelengths were obtained by the formation of an n^+ region on the light incident side while the array with a high recombination velocity had an untreated etched surface. In the near infrared (wavelengths $>$ 0.90μ) the thicker array had a higher response. This is not surprising

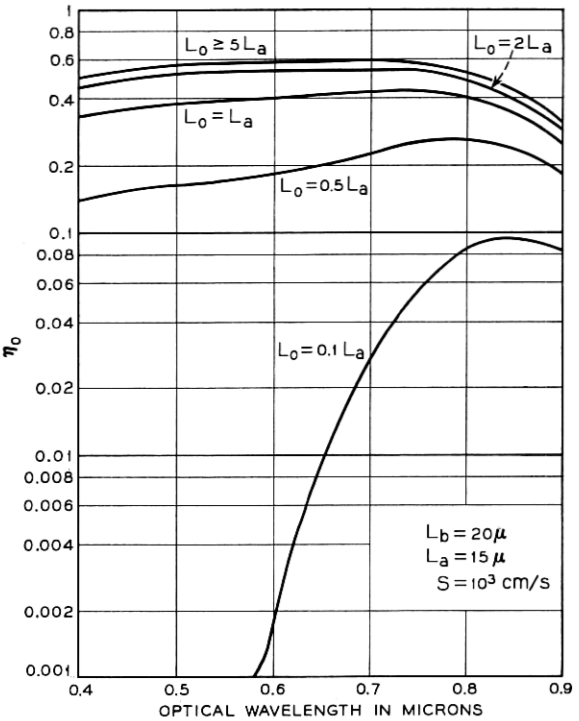

Fig. 6 — Calculated plots of η_0 versus optical wavelength for different values of minority carrier lifetime or equivalently different values of the diffusion length L_0 and for a low value of surface recombination velocity S.

since the only reason η_0 is falling with increasing wavelength in this range is because the photon energy is approaching the bandgap energy of silicon and the substrate is becoming transparent.

The sensitivity of a diode array camera tube is compared with that of a commercially available vidicon and the response of a unity quantum efficiency ($\eta_0 = 1$) ideal detector is shown in Fig. 9a. The target of the diode array tube was approximately 20μ thick and had a low recombination velocity on the light incident surface. For the comparison, both tubes were operated with comparable dark currents. The dark current of a typical diode array camera tube is in the range from 5 to 50 nanoamperes. This upper value of dark current is obtained at a target bias of 30 volts in a typical vidicon with visible light response. The vidicon response curves shown in Figure 9 were obtained with this target bias. The light power incident on the tubes was adjusted so

that the video output current was approximately equal to the dark current. The conclusion that follows from the curves given in Fig. 9a is that the diode array camera tube has a much broader and a much higher sensitivity than that of a vidicon.

The sensitivity of the diode array camera represented by the curve given in Fig. 9a may also be expressed as approximately 20 μamps per ft-cd of faceplate illumination when the scene is illuminated with an incandescent lamp operating at a normal temperature. The corresponding response of a vidicon with 50 nanoamperes of dark current may be written as approximately 0.6 μamp per ft-cd at a faceplate illumination of 0.1 ft-cd. At this light level, the video signal current of the vidicon is comparable to that of the dark current; because of the photoconductive decay characteristics the image lag in the displayed video may be excessive. For fluorescent illumination the

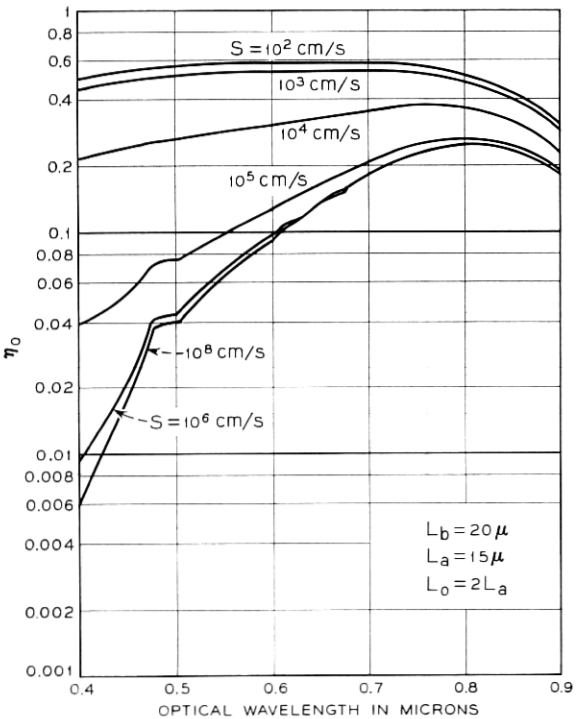

Fig. 7 — Calculated plots of η_0 versus optical wavelength for various values of surface recombination velocity.

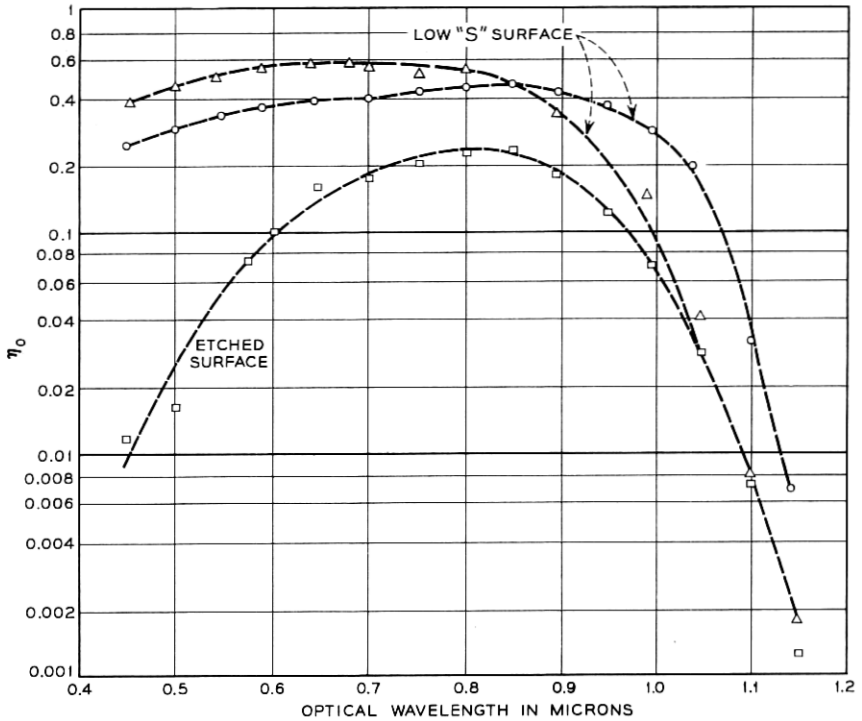

Fig. 8 — Measured values of η_o as a function of optical wavelength for different substrate thicknesses and for targets with a low and high (etched) surface recombination velocity at the light incident surface. *Target Thickness:* ○ Approximately 4.3 mils, △ Approximately 1.0 mils, and □ Approximately 1.0 mils.

sensitivity of the diode array camera is approximately 1.3 μamps per ft-cd of faceplate illumination.

The sensitivity of a vidicon is less at higher levels of illumination since its gamma is approximately 0.65. This is ilustrated in Fig. 9b in which the sensitivity versus output signal current is plotted for a diode array camera tube and a vidicon. These curves were obtained with monochromatic illumination at a wavelength of 0.55μ when both tubes were operated at a dark current of approximately 0.02 μamp. The zero slope of the diode array camera tube results from a unity gamma; whereas the slope for the vidicon corresponds to the value of $(\gamma - 1)$.

The cross-hatched area below 0.02 μamp of output signal current is the region where the dark current is greater than the signal cur-

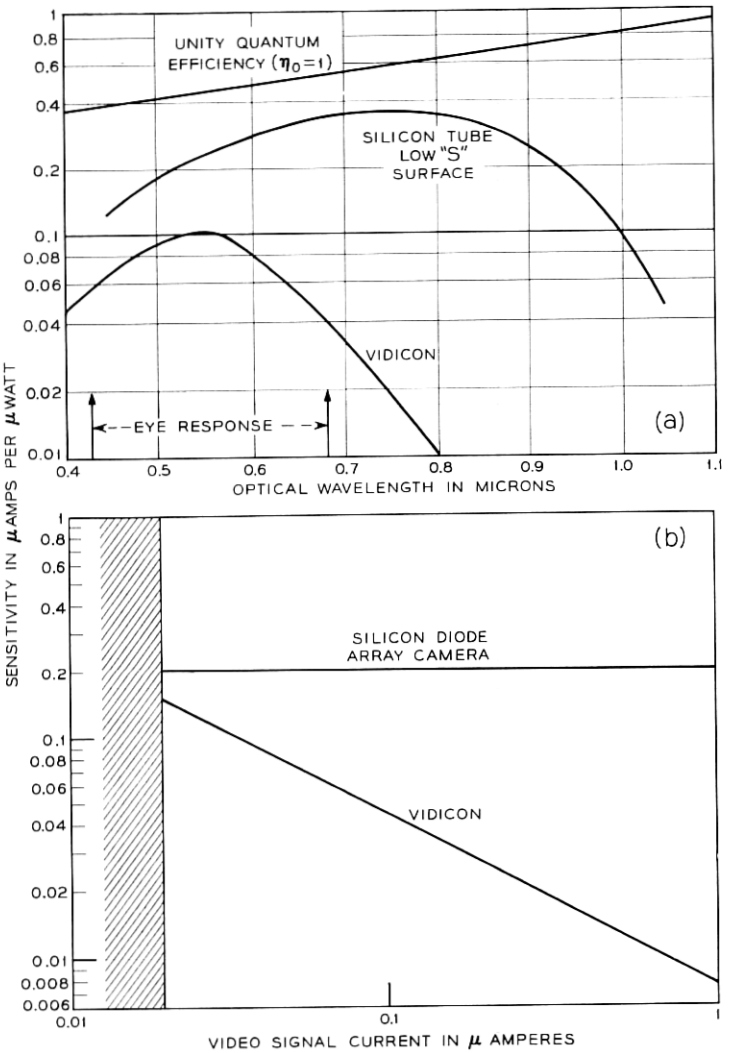

Fig. 9 — (a) Sensitivity of a silicon diode array camera tube as a function of optical wavelength. As a comparison the sensitivity of a commercially available vidicon is also plotted. For the vidicon the signal current was equal to the dark current (0.05 μa) at all wavelengths. (b) Sensitivity of a silicon diode array camera and a vidicon as a function of video signal current: Optical wavelength $= 0.55\ \mu$; dark current $= 0.02\ \mu$ amps.

rent and is considered to be below the operating range of both camera tubes. As the signal current approaches 1.0 μamp, the sensitivity of a vidicon is reduced to a value approximately 1/25 of a diode array camera tube. Notice that the optical wavelength of 0.55μ used for the above comparison corresponds to the peak of the response for both the vidicon and the normal eye.

For the experimental curves of Fig. 8 no effort was made to reduce the reflectivity of the substrate below that given in Fig. 4 for bare silicon which is approximately 0.34 throughout the visible portion of the spectrum. This reflectivity can be significantly reduced by a single-layer antireflection film. As illustrated by the dotted curve of Fig. 4, a film of evaporated silicon monoxide, 550 Å thick, will reduce the reflectivity to less than 0.10 throughout the visible portion of the spectrum. When such a film is used on a diode array target, the target sensitivity is increased by an amount corresponding to the reduction in reflectivity for wavelengths greater than approximately 0.55μ. For wavelengths less than 0.55μ, the sensitivity is also increased but not as much as would be expected from the reduction in reflectivity. The reason is not fully understood but it may be that light absorption in the evaporated silicon monoxide layer is appreciable at these shorter wavelengths.

In the diode array camera, the video signal is normally obtained from the target lead as in a conventional vidicon; as a result, the lowest usable light level will be determined by thermal noise sources in the video preamplifier. This means that in spite of the high sensitivity of the basic silicon diode array camera, its use will be restricted to relatively bright light with presently available commercial preamplifiers. If it is desired to operate at extremely low light levels, the use of return beam reading with secondary emission amplification may improve matters. The minimum detectable light level of an image tube depends upon a number of factors, and the actual determination of this level is beyond the scope of this paper. With return beam reading, however, the minimum detectable light level of the silicon diode array camera would probably be limited by the presently achievable room temperature dark current of 5 to 50 nanoamperes.[18] A modest amount of cooling could be used to reduce the dark current considerably since the dark current drops an order of magnitude for a reduction in temperature of about 25°C.

Consider how lateral diffusion of the photo-generated holes affects the resolution capabilities of the model depicted in Fig. 3. The resolution capabilities of a camera tube are usually evaluated by illuminat-

ing the tube with a sinusoidal light pattern, measuring the peak-to-peak video response as a function of the spatial wavelength or frequency of the light pattern, and normalizing with respect to the response for uniform light. For targets with low values of diode leakage currents it is reasonable to assume that the peak-to-peak video signal is proportional to the peak-to-peak hole flux entering the p-region of Fig. 3. Therefore, the modulation transfer function resulting from the hole diffusion process, R_D, is readily obtained from equation (4), the result is

$$R_D(k) = \eta_k/\eta_o .$$

Values of R_D for various values of the target parameters can be obtained from equation (5).

The response $R_D(k)$ will be a function of the wavelength of the incident light pattern, increasing with increasing wavelength as long as multiple reflections in the substrate are not significant. This increase results from the fact that at the longer wavelengths more of the photo-generated holes are created closer to the edge of the depletion region and thus they do not have as far to diffuse. In addition, the existence of a dead layer and associated electric field may result in greater resolution capabilities than predicted by equation (5) when the illumination is restricted to wavelengths less than 0.5μ.

As illustrated by Fig. 10, where R_D is plotted versus spatial frequency $(k/2\pi)$ for various values of L_b, the degradation in resolution contributed by lateral diffusion is a strong function of target thickness. For these curves the width of the depletion region $(L_b - L_a)$ was kept constant at a value of 5μ and the wavelength of the incident light was assumed to be 0.55μ. The quantity $R_D(k)$ will also be a decreasing function of the minority carrier lifetime τ. This is illustrated by the curves of Fig. 11 for which τ has been increased an order of magnitude over the value used for Fig. 10. For the curves of both of these figures a low surface recombination velocity was used because this is a necessity for adequate sensitivity in the visible portion of the spectrum. The resolution and sensitivity will be relatively independent of τ or L_o when $L_a \ll L_o$. However, if $L_o < L_a$, then the sensitivity will increase and the resolution will decrease with increasing L_o, and vice versa.

3.2 *Image Detection with a Mosaic*

The discrete nature of a diode array target places a limit on its resolution capabilities; an estimate of this limit can be obtained if the model depicted in Fig. 3 is modified so that the homogeneous

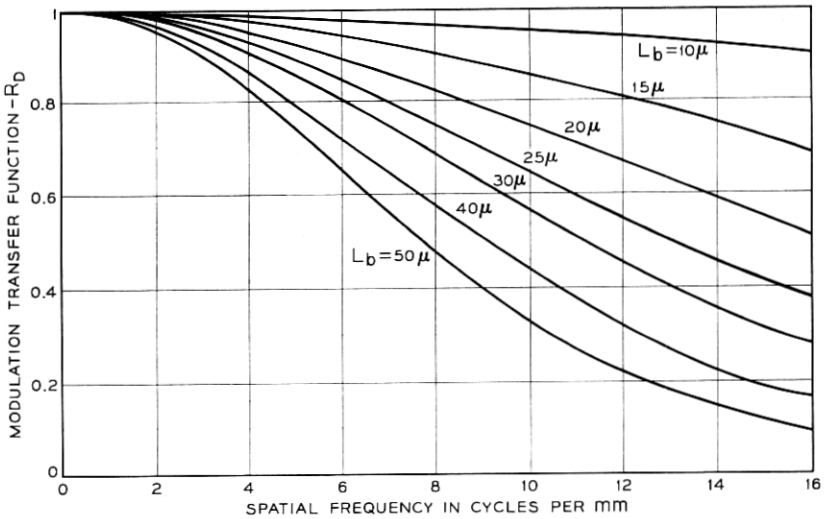

Fig. 10 — Calculated values of the modulation transfer function resulting from lateral hole diffusion, R_D, as a function of spatial frequency for various values of target thickness, L_b, and for a minority carrier lifetime corresponding to a diffusion length of 15μ. (L_a = 15μ; S = 10^3 cm/s; $L_b - L_a$ = 5μ; optical wavelength = 0.55 μ)

p-region is divided into discrete p-islands as indicated in Fig. 12. It will be assumed that the lateral conductivity of each p-type island is infinite.

The resolution capabilities of the mosaic will be obtained by evaluating the peak-to-peak response obtained on the p-type islands for a given incident hole flux. The response of the nth island r_n will be proportional to the total number of holes collected by this p-region; if $J'_p(x)$ is the hole flux, then

$$r_n \propto \int_{(n-1)d_p}^{(n+1)d_p} J'_p(x)\, dx \tag{6}$$

in which $2d_p$ is the center-to-center spacing of the islands. Assuming a sinusoidal variation in the incident light pattern, it follows from equation (4) that

$$J'_p(x) = (N_0/2)[\eta_0 + \eta_k \cos(kx + \varphi)] \tag{7}$$

where φ is a spatial phase factor that accounts for the relative orientation between the mosaic and the light pattern. The peak-to-peak response will be a function of the phase relationship φ between the

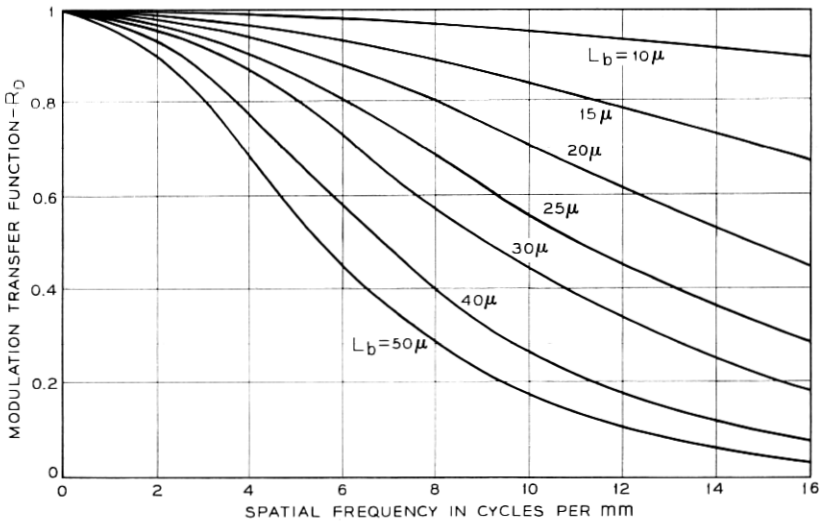

Fig. 11 — Calculated values of the modulation transfer function caused by lateral hole diffusion R_D as a function of spatial frequency for various values of target thickness L_b and for a minority carrier lifetime ten times that used for Fig. 10. ($L_a = 47.3\mu$; $S = 10^3$ cm/s; $L_b - L_a = 5\mu$; optical wavelength 0.55μ)

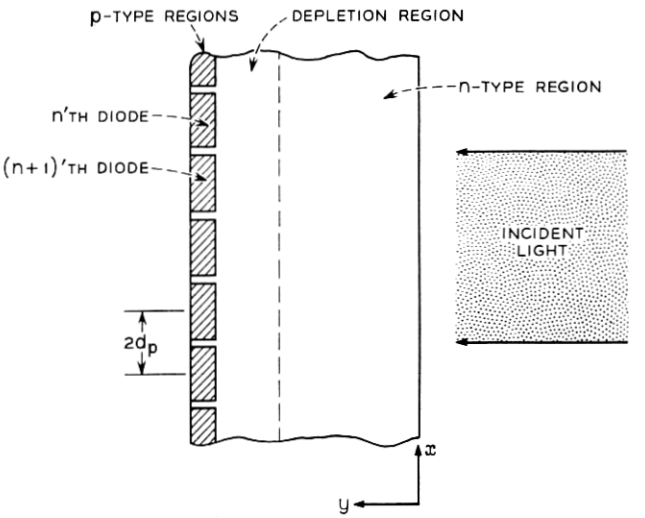

Fig. 12 — Model used to estimate the loss in resolution caused by the finite diode spacing.

light pattern and the mosaic; however, if we restrict our considerations to spatial wavelengths greater than two or three times d_p, the response will be virtually independent of φ. With equation (6) and (7), the peak-to-peak response of the mosaic can be evaluated and if this is normalized with respect to the response for uniform light, the resulting modulation transfer function $R(k)$ is given by

$$R(k) = \frac{\eta_k}{\eta_0}\left(\frac{\sin kd_p}{kd_p}\right) = R_D(k)\left(\frac{\sin kd_p}{kd_p}\right) \qquad \text{for} \quad kd_p \ll 2\pi. \tag{8}$$

Thus because of the discrete nature of the diode array target, its resolution capabilities are reduced by the factor

$$\sin kd_p/kd_p\,.$$

The effect of this function on the curve of Fig. 10 corresponding to $L_b = 20\mu$ is shown in Fig. 13 for various values of the diode spacing $2d_p$.

In addition to lateral diffusion and the discrete nature of the target, the resolution capabilities of an operating camera tube will be degraded by the finite size of the electron beam. Measured modulation

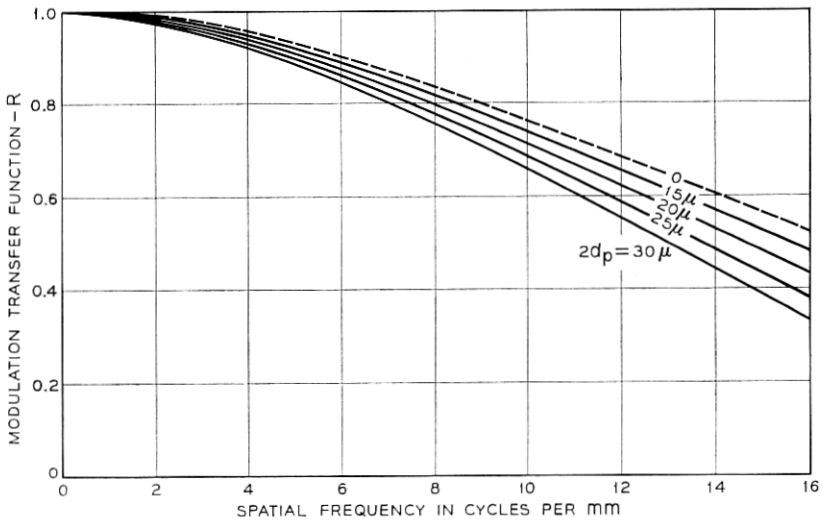

Fig. 13 — Calculated values of the modulation transfer function due to lateral hole diffusion and the finite diode spacing as a function of spatial frequency for various diode spacings. ($L_b = 20\mu$; $L_a = 15\mu = L_e$; $S = 10^3$ cm/s; optical wavelength $= 0.55\mu$).

transfer functions of a typical diode array camera tube for electrostatically and magnetically focused electron beams are given in Fig. 14. Using reasonable estimates of the unknown target parameters, the modulation transfer function can be calculated from equation (18); the results of such a calculation are also given in Fig. 14. The agreement between calculation and experiment is fairly good when a magnetically focused electron beam is used. The increased resolution obtained with magnetic focus compared with electrostatic focus results from a smaller electron beam size.

IV. MODIFICATIONS OF THE BASIC TARGET STRUCTURE

In the basic diode array structure, the silicon dioxide is exposed directly to the scanning electron beam; it has been found that sufficient negative charge can accumulate on the insulating silicon dioxide layer to prevent the beam from striking the recessed p-type islands. The effect of the silicon dioxide film is analogous to that of a control grid in a triode. This section discusses three modifications of the basic diode array structure that will prevent this charging behavior and will improve the performance of the array in other respects.

4.1 *Enlarged Islands*

One modification of the basic diode array structure, identified as a conducting island structure, is shown in Fig. 15. In this structure, electrically isolated conducting islands are placed over each p-type region. If the spacing between islands is small enough, most of the silicon dioxide film will be covered with a conducting material so that charging of this surface should be reduced if not eliminated.

Another advantage of the island structure is that the electron beam current is utilized more efficiently. With the typical diode spacing of 20μ and the typical diode diameter of 8μ only approximately $\frac{1}{8}$ of the total beam current is available for producing an output signal if beam pulling effects are neglected. This is simply the ratio of the total exposed area of all of the p-regions to the total target area. With the conducting islands, the beam landing area of each p-type region is greatly increased and more of the beam current can be used. Reducing the required beam current permits smaller beam diameters to be achieved and as a result the degradation in resolution because of the size of the electron beam may be reduced and possibly the cathode loading may be reduced.

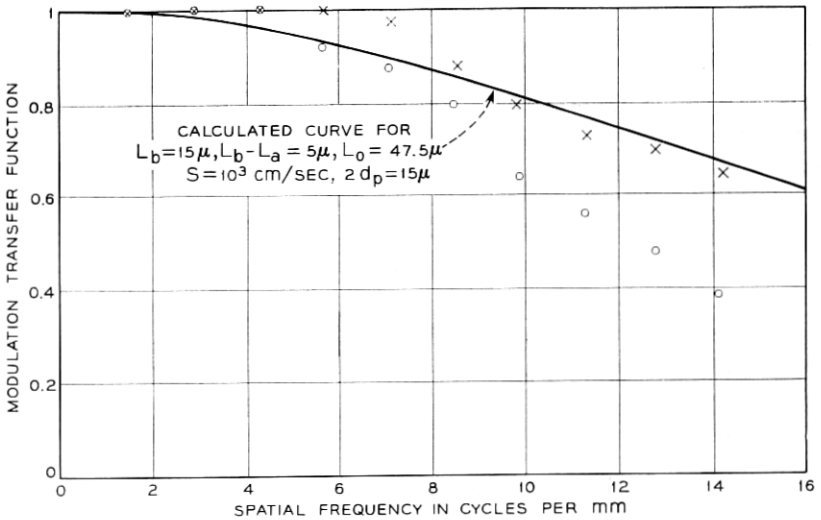

Fig. 14 — Measured values of the modulation transfer function of a diode array camera tube as a function of spatial frequency. Results are given for both a magnetically (x) and electrostatically focused (o) electron beam (optical wavelength = 0.55μ).

The conducting islands will also increase the capacitance shunting the diodes without a corresponding increase in the diode leakage current. Thus the time constant and the charge storage characteristic or dynamic range of each diode will be increased. However, this increase in capacitance must be consistent with the image lag requirements because if the capacitance becomes too large the electron beam may not be able to fully recharge the diode in one scan.

Another potential advantage of metallic conducting islands is that the infrared sensitivity will be increased at wavelengths where a significant amount of light can pass through the substrate. The metallic islands will reflect most of the transmitted light back into the substrate and thus effectively double the absorption path. Furthermore, the metallic islands will also shield the substrate from stray light emitted by the cathode.

Several diode array camera tubes with gold conducting islands have been fabricated. The thickness of the gold islands was about 0.5μ; the minimum separation between islands that has been successfully achieved to date is approximately 3μ. These arrays when examined in a camera tube still showed significant charging effects. These

results indicate that with an island thickness of approximately 0.5μ, an island separation of less than 2μ would be required to eliminate the charging behavior. However, stringent requirements must be placed on the photolithographic processes in order to obtain this small separation over the entire array. On the other hand, if the thickness of the islands is considerably increased, it might be possible to use a larger island separation with no deleterious charging effects.

4.2 *Conductive Sea Surrounding the p-Type Islands*

Another attractive target structure, called a conducting sea structure, is illustrated in Fig. 16. In this embodiment the silicon dioxide is covered by a conducting material which surrounds the diodes without contacting the p-type islands. This structure should also eliminate charging effects since the silicon dioxide is shielded from the electron beam.

An attractive feature of the conducting sea is that the potential between the sea and the n-type substrate can be varied. Thus the silicon surface potential at the silicon-silicon dioxide interface can be controlled and, more important, it can be optimized so as to minimize the leakage current resulting from generation centers at the interface. These centers are the dominant source of dark current in an operating camera tube. Notice that the capacitance between the sea and the substrate is rather large (approximately 6000 pF per cm^2 for an oxide thickness of 0.5μ, assuming no depletion at the interface), and the

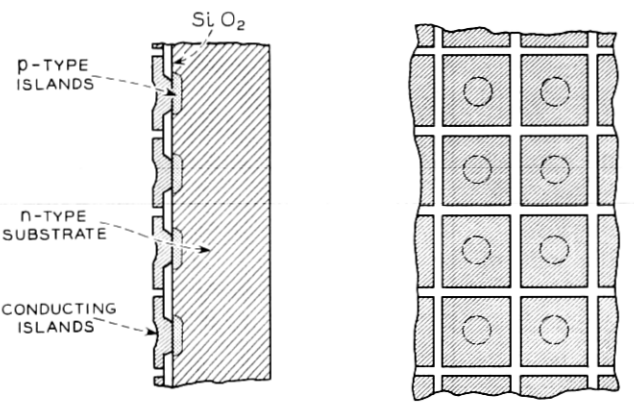

Fig. 15 — Conducting island structure in which electrically isolated conducting islands are placed over each p-type region.

high frequency shunting effects of this capacitance must be reduced by the use of a high frequency blocking filter in the bias lead for the sea as shown in Fig. 16.

The conducting sea also has the potential advantage of providing electronic gain. Gain may be obtained by adjusting the bias applied to the conductive sea so that the fraction of beam current which can strike the sea will be modulated by the charge pattern stored on the p-type islands. The video signal is obtained from the parallel combination of the conductive sea and the n-type substrate. When the target is operated in this mode, the performance should be similar to a triode with zero spacing between the control grid and the plate.

The practicality of these advantages depends upon the development of successful fabrication techniques for creating the conductive sea. Thus far inadvertent shorts between the sea and the substrate or between the sea and some of the p-type islands have prevented actual evaluation of a conducting sea structure.

4.3 *Resistive Sea in Contact with the p-Type Islands*

Another technique for eliminating the uncontrolled charging of the silicon dioxide film is illustrated in Fig. 17. In this case, a resistive film or sea covers both the silicon dioxide film and the p-type islands. This resistive sea prevents any build-up of excess charge in the regions between p-type islands by providing a controlled leakage path to the individual diodes. The resistance (that is, ohms per square) of the resistive sea must be chosen judiciously in order to provide this leakage path without impairing the resolution capabilities of the basic diode array target. This implies that there should not be a significant amount of charge leakage between picture elements during a frame period (that is, 1/30 second).

Section V shows that for a silicon dioxide film thickness of approximately 0.5μ, the resistivity of the resistive sea must be greater than approximately 10^{13} ohms per square. This sheet resistivity has been obtained with thin films formed by evaporation or sputtering. Table I lists some of the source materials that have been tried. Since sometimes the process was performed in the presence of a background gas, the composition of the resulting resistive film is not precisely known. The required film resistivity is rather high and one of the biggest problems in obtaining suitable resistive sea structures has been reproducibility. Comments about the reproducibility of the different materials are given in Table I.

Although in many respects Sb_2S_3 works well as a resistive film, it

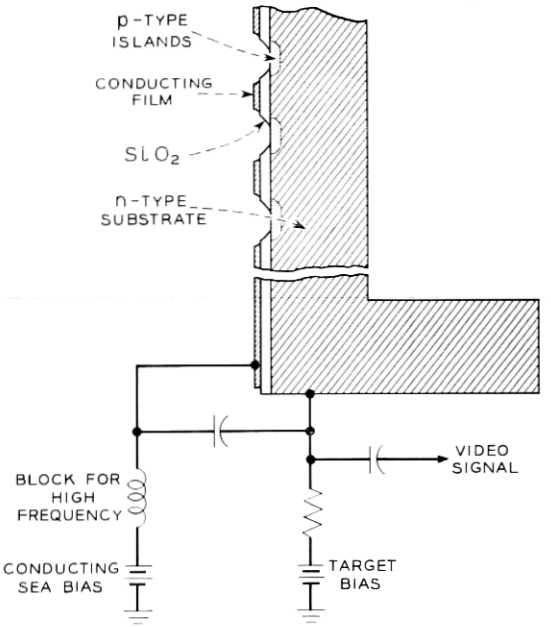

Fig. 16 — Conducting sea structure with suitable bias network. In this structure, the silicon dioxide surrounding the *p*-type islands is covered with a conducting material.

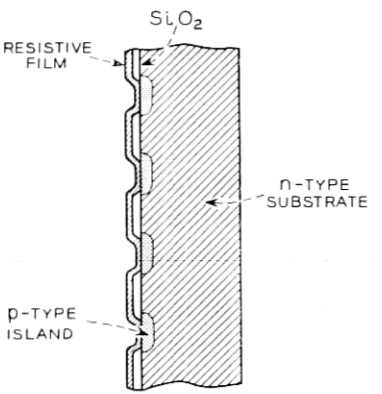

Fig. 17 — Resistive sea structure.

TABLE I—SOURCE MATERIALS

Material	Method of deposition	Obtainable resistivity	Reproducibility
Sb_2S_3	Evaporated	High enough	Small problem
GaAs	Evaporated	High enough	Problem
SiN*	Sputtered	High enough	?
Si*	Evaporated Sputtered	Marginal	Extreme problem
Ha (Ta) N†	Sputtered	High enough	?

* These films were provided by E. N. Fuls.
† This film was provided by F. Vratny.

has one serious drawback. That is, the completed camera tubes with an Sb_2S_3 film cannot be vacuum baked at high temperature. The other materials listed in Table I result in films which permit the camera tube to be baked at 400°C.

Of the many structures and techniques proposed to eliminate the charging problem associated with the basic diode array structure, we have found the resistive sea structure to be the simplest to implement and to date it has given the best results. All of the experimental results presented in this paper were obtained with diode arrays which had a resistive sea.

V. RESISTIVE SEA STRUCTURE

It is quite clear that a resistive film covering the diodes and the silicon dioxide can affect the resolution capabilities of the basic diode array structure and, as pointed out previously, in order for the film not to impair these capabilities, its resistance should be such that there is not a significant amount of charge leakage between picture elements during a frame period. In addition to affecting the resolution, the amount of lateral charge spreading permitted by the film during a frame period will influence many of the other electrical properties of the basic diode array structure.

The following model of the resistive film will be used to establish the required sheet resistivity and to provide a basis for interpreta-

tion of experimental results. It will be assumed that the film can be characterized by an effective sheet resistance R_f. This sheet resistance could be a function of the free carrier density spatial distribution in the film if the current flow is space charge limited or if interface states are present at the oxide-film interface. To simplify the present considerations, we assume that R_f is independent of the lateral current flow in the film and that the free carriers in the film are negatively charged and reside at the oxide interface.

Under these assumptions the voltage distribution with respect to the cathode V on the resistive film as a function of time will satisfy the following equation

$$\nabla^2 V = R_f C \frac{\partial V}{\partial t} \tag{9}$$

in which C is the capacitance per unit area between the oxide-film interface and the substrate. This capacitance, which consists of the series combination of the oxide capacitance and the capacitance of the depletion region formed at the oxide-silicon interface, will generally be a function of the difference between the substrate voltage and the film voltage. To obtain a model amenable to analysis the capacitance C will be assumed to be independent of V. This assumption will be valid for a target in an operating camera tube if the maximum amplitude of V is small compared with the target (substrate) voltage.

To obtain some idea of the minimum film resistivity or charge spreading behavior required to prevent a loss in resolution, consider a simple model of the resistive sea structure that neglects the discrete nature of the target. The oxide layer is assumed to be uniform in the lateral direction as indicated in Fig. 18. With such a model, it is possible to determine, for a given stored charge pattern, a minimum

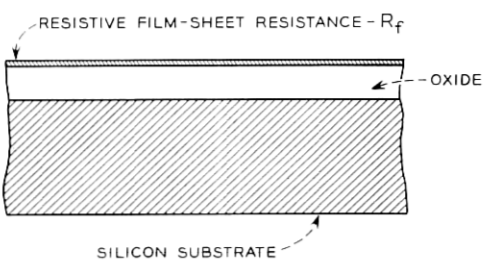

Fig. 18 — The model used for analyzing the resistive sea structure.

value for R_f for which there is no appreciable lateral charge leakage during a frame time.

Since the purpose of the resistive film is to provide a controlled charge leakage path without introducing a concurrent loss in resolution, the decay rate of a given initial charge distribution is the parameter of interest. If we restrict our considerations to a one dimensional charge distribution and a uniform oxide layer, equation (9) becomes

$$\frac{\partial^2 V(x, t)}{\partial x^2} = R_f C \frac{\partial V(x, t)}{\partial t} \tag{10}$$

in which x is a lateral coordinate parallel to the film.

Let the initial charge distribution at the resistive film-oxide interface be given by

$$q_k(x, t = 0) = q_0 \cos kx$$

in which

$$k = 2\pi(\text{spatial wavelength})^{-1}.$$

This charge distribution will create a voltage profile which may be approximated as

$$V_k(x, t = 0) = (q_0/C) \cos kx,$$

provided $k \ll C/\epsilon_o$, where ϵ_o is the permittivity of free space. It follows from equation (10) that such an initial voltage profile will decay exponentially with time with a time constant τ_k that is given by

$$\tau_k = R_f C/k^2. \tag{11}$$

Thus the time interval over which a sinusoidal charge pattern may be stored without smearing is proportional to the square of the spatial wavelength of the pattern.

If the decay time of the voltage profile is required to be 10 times the frame period of 1/30 second so that there is only a 10 percent loss in resolution resulting from charge spreading, then the value of R_f must be such that

$$R_f > k^2/3C.$$

For a spatial frequency of 14 cycles per mm, the largest spatial frequency of interest, and assuming $C \cong 4000$ pF per cm^2 (a value which lies between the oxide capacitance and the capacitance of the depletion

region under the oxide), it follows that

$$R_f \gtrsim 5 \times 10^{13} \text{ ohms per square.}$$

This implies that for a resistive sea thickness of approximately 0.1μ, a bulk resistivity of at least 10^8 ohm-cm is required for the material of the resistive layer.

Measurements of the decay of an initial voltage distribution have been used to obtain estimates of the sheet resistances of the resistive films. A voltage distribution is created on the resistive sea by focusing onto the camera target a bar pattern (resolution chart) that is illuminated by a light pulse, the duration of which is much shorter than a frame period. The light induced charge pattern and resulting voltage pattern is introduced to the resistive film in discrete areas corresponding to the p-regions of the diodes. If the spatial wavelength of the illuminated bar pattern is much greater than the diode spacing, then the charge over the p-regions will relax into the surrounding areas in a time that is short compared with the relaxation time of the overall light induced charge pattern. For times longer than the relaxation time between diodes, the simple model discussed above should be valid. In the measurements, the peak-to-peak video response is measured as a function of the time between when the bar pattern is illuminated with the light pulse and when the electron beam scans the light induced charge pattern produced on the resistive sea.

Some results obtained from this type of measurement are given in Fig. 19 for targets with different film resistances. During the time between writing and reading, the electron beam was blanked so that no electrons were hitting the target. A square wave bar pattern was used and the dotted lines are calculated curves for the decay of an initial square wave voltage profile using the simple model discussed above. Except for very short times, the agreement between calculation and experiment is very good. At long enough times, only the fundamental component of the square wave contributes to the video signal and the decay is then truly an exponential, that is a straight line on the semilog plot of Fig. 19. The sheet resistances indicated in the figure were calculated from the decay times of the various curves by assuming the effective capacitance between the film and the substrate was the same for all curves and was equal to 4000 pF per cm^2. In the remainder of the paper, when a value of sheet resistance is given, it refers to a value obtained from decay curves as plotted in Fig. 19.

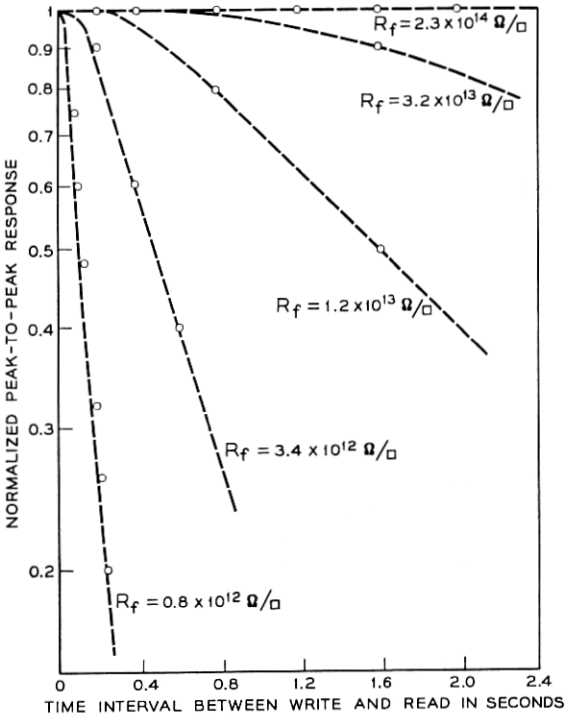

Fig. 19 — Peak-to-peak video response obtained from a bar pattern as a function of the interval between the time when the bar pattern is optically written onto the target with a light pulse and the time when the pattern is read with the electron beam. During the interval between writing and reading the electron beam was not scanning the target. The various curves are for different film resistances. (Spatial wavelength = 0.04 cm; C = 4,000 pF/cm^2) ○ experimental points, --- calculated curves.

It has been found that targets with low resistivity films (sheet resistances $<10^{13}$ ohms per square) will have certain distinguishing characteristics that are quite different from those observed on targets with high resistivity films (sheet resistances $>10^{14}$ ohms per square). That is, the resistance region between 10^{13} ohms per square and 10^{14} ohms per square is a transition region for the typical diode arrays with a diode spacing in the range of 15 to 20μ. One of the most striking contrasts between targets with a high resistivity film and those with a low resistivity film occurs when the video current through a white defect is observed as the substrate voltage is increased. Most arrays fabricated to date have isolated diodes which exhibit higher values of dark

current than their neighboring diodes. This higher value of dark current manifests itself in the displayed video as an isolated bright spot or equivalently a white defect.

The behavior of a target with a low resistivity film is illustrated in Fig. 20. The pictures in this figure are of the video display of the dark current pattern at different target voltages obtained from a camera tube which had many white defects. With the low resistivity film, as the target voltage is increased, the video current through the defects increases, that is, the white spots get brighter and also tend to enlarge only slightly.

Compare this behavior with that exhibited by a target with a high resistivity film as shown in Fig. 21. Here, as the target voltage is increased the video current through the defects again increases, but now when the target voltage reaches a certain critical voltage, the

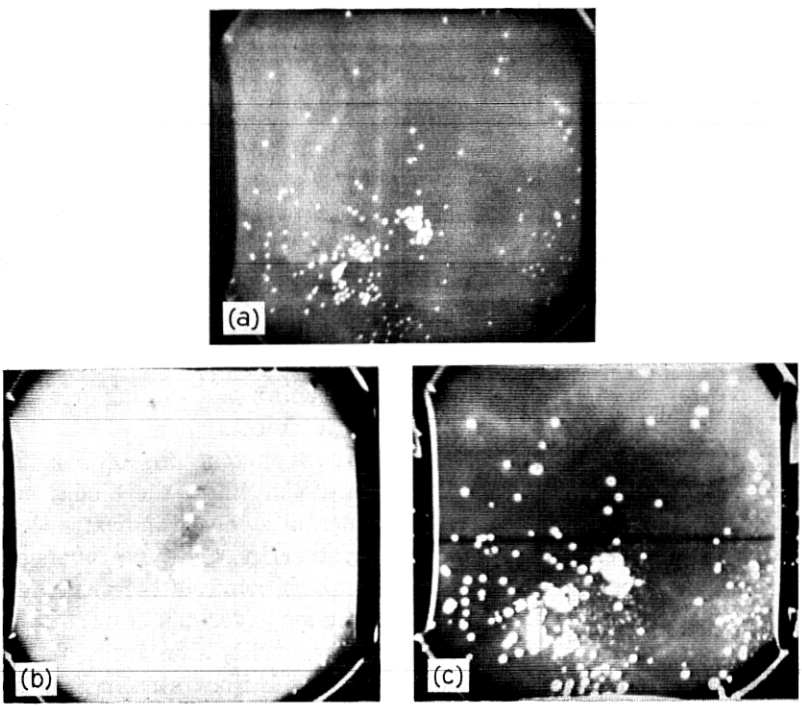

Fig. 20 — Photographs of the video display of the dark current pattern at different target voltages obtained from a camera tube in which the target had a low resistivity resistive film: (a) $V_T = 1.5$ volts, (b) $V_T = 5.0$ volts, (c) $V_T = 12$ volts. (Video display scan lines and printing screens cause moiré patterns in some figures that are not in the originals.)

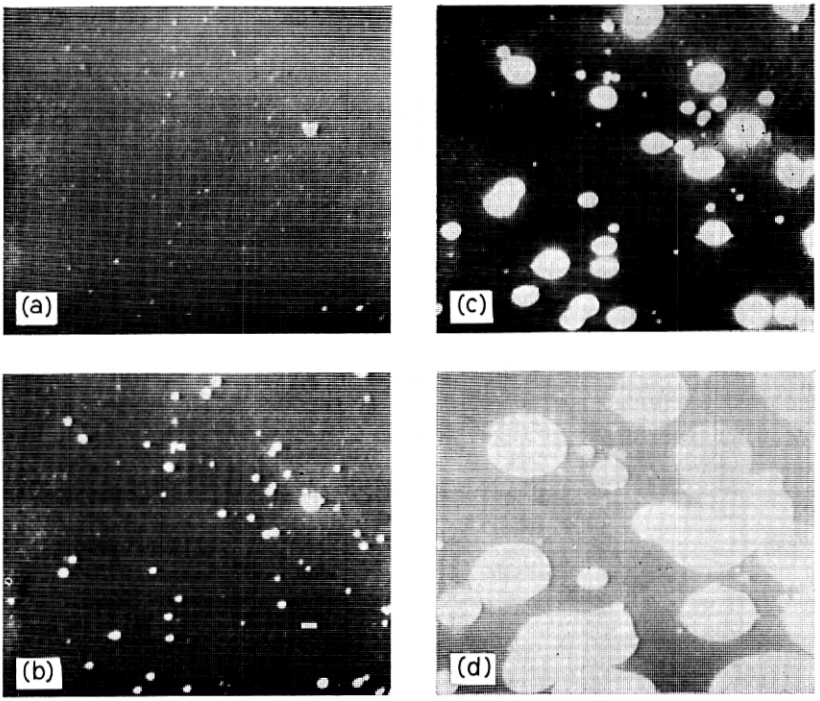

Fig. 21 — Photographs of the video display of the dark current pattern at different target voltages obtained from a camera tube in which the target had a high resistivity resistive film: (a) $V_T = 2.5$ volts, (b) $V_T = 3.0$ volts, (c) $V_T = 3.5$ volts, (d) $V_T = 4.0$ volts.

defects grow larger in the lateral direction very rapidly and eventually envelop the entire target. This enveloping or "whiting out" of the target can result from only one single defect.

The large white regions in the last two photographs of Fig. 21 cover many diodes and correspond to areas in which the diodes are all electrically shorted together. Experimental evidence indicates that these diodes are electrically shorted together by a p-type inversion layer which forms under the oxide and which connects the originally isolated p-regions. The fact that an inversion layer can form with a high resistivity film but not with a low resistivity film turns out to be what one would expect; the reason for this is illustrated in Fig. 22.

In the top part of the figure, the area around one diode is schematically indicated just after the electron beam has recharged the diode. The film potential will be at cathode potential; assuming the target voltage or the potential of the n-region is high enough, ap-

proximately 5 to 8 volts for a 10 Ω-cm substrate and an oxide thickness of approximately 0.5μ, the area under the oxide will also be depleted as indicated. Let us further assume that in the vicinity of this diode there is for some reason a high generation rate of minority carriers. This situation could arise for example as the result of some sort of defect in the vicinity of the diode.

The charge collected on the p-region resulting from the large generation rate will cause both the potential of the p-type island and the potential of the film over the p-region to increase from cathode potential towards target potential. What happens now depends upon the charge spreading behavior of the film.

As indicated in the lower left half of Fig. 22, the rise in potential of the p-type region for a low resistivity film will be communicated laterally a significant distance during a frame period. Thus the film potential over the oxide increases and as a result both the diode depletion region and the depletion region under the oxide directly surrounding the

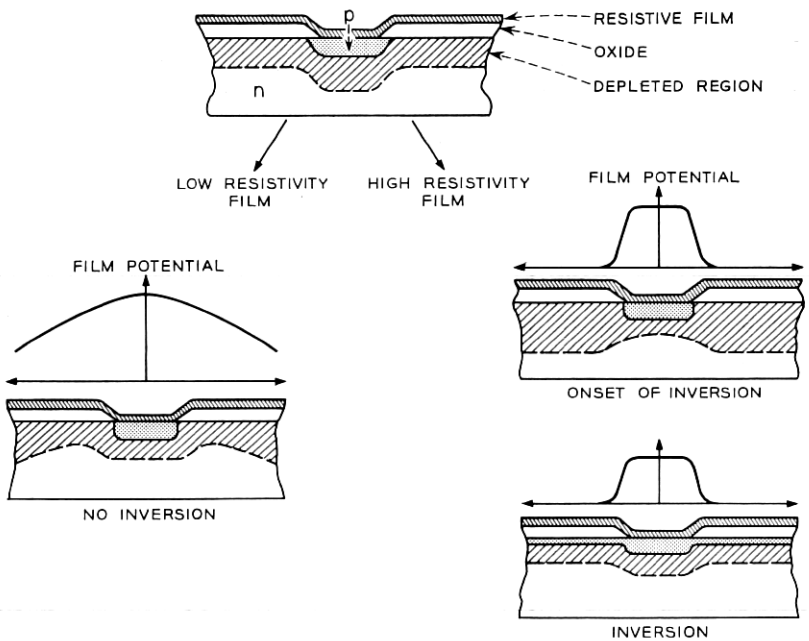

Fig. 22 — Illustration of how an inversion layer can form around a defect when a high resistivity resistive film is used but not when a low resistivity resistive film is used.

p-region will be reduced. The reduction of the depletion region under the oxide inhibits the formation of an inversion layer and no inversion occurs in this case.

On the other hand, as indicated in the lower right half of Fig. 22, with a high resistivity film the rise in potential of the p-region is not accompanied by a rise in potential of the film out over the oxide. Therefore, the depletion region under the oxide will not immediately collapse along with the diode depletion region and an electric field in the lateral direction will be produced which forces holes from the p-region into the depletion region under the oxide, resulting in the formation of an inversion layer. As the experimental results have indicated, the inversion layer can cause many diodes to be shorted together. This behavior is similar to the shorting together of the source and drain of an insulated gate field effect transistor by the application of the appropriate voltage to the gate electrode.

Thus with a high resistivity film we have the possibility of inversion layers forming at a defect whereas with a low resistivity film the lateral charge spreading inhibits the formation of an inversion layer.*

Besides influencing the target properties discussed above, the resistive sea also affects the ability of the electron beam to re-establish the full value of the reverse bias on a diode during one scan.[15] Some insight into this problem can be obtained from the equivalent circuit shown in Fig. 23 which approximates one of the diodes. In this figure the p-n junction is represented by a schematic diode which is shunted with an effective junction capacitance, C_j, and a current generator. The equivalent circuit is valid only if the charge stored on the oxide surrounding the diode is negligible compared with that stored on the diode. The resistive sea immediately over the p-region is represented by the parallel combination of R_s and C_s. The time-constant for this combination is the intrinsic time-constant for the resistive sea (that is, $R_sC_s = \rho_s\epsilon_s\epsilon_o$ where ϵ_s is the relative dielectric constant and ρ_s is the volume resistivity of the resistive film).

A qualitative estimate of the charge storage properties of the

---

* These conclusions are consistent with the results obtained by Grove and Fitzgerald[19] on a gate-controlled diode structure. They show that for inversion to occur, the difference between the silicon surface potential at the oxide interface and the reverse bias voltage of the diode must be less than twice the fermi potential of the substrate. Because of the lateral charge spreading in a low resistivity sea, this inequality is never satisfied whereas with a high resistivity sea it can be satisfied in a region where there is a high generation rate of minority carriers.

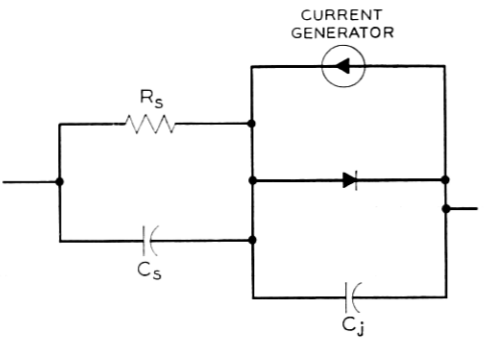

Fig. 23 — Equivalent circuit used to represent the area around one diode or p-type region.

equivalent circuit can be obtained from intuition. Consider first the fact that the electron beam will charge both the resistive sea and the beam side of capacitor C_s down to zero potential. If the reverse-bias leakage current of the diode may be neglected, the resistor R_s will discharge any voltage difference across C_s at a rate related to the time-constant R_sC_s. From the previous discussion it is estimated that ρ_s is approximately 10^8 ohm-cm. Therefore, R_sC_s may be estimated to be 35 μsec by assuming ϵ_s to be 4. Thus, without illumination, the p-regions are quickly charged to cathode potential and the full value of reverse-bias is placed across the diode.

The current from the photoresponse is represented by the current generator in Fig. 23. Since the capacitance from the film surface to electrical ground is very small, any change in reverse-bias voltage across the diode caused by photoresponse throughout the frame period appears very quickly on the electron beam side of the resistive sea. Furthermore, this process does not create a significant voltage drop across R_s. However, when the full value of reverse bias is re-established by the scanning electron beam, a significant voltage drop may appear across the parallel combination of R_s and C_s since the beam is on a diode for less than 0.3 μsec. For example, if the photoresponse has created a reduction in diode reverse-bias of ΔV_1 volts, the process of charging the beam side of the resistive sea down to zero volts will increase the reverse-bias by the amount ΔV_2 where

$$\Delta V_2 = \frac{C_s}{C_s + C_j} \Delta V_1.$$

The ratio of ΔV_2 to ΔV_1 may be estimated by assuming equal values

for the relative dielectric constants for the resistive sea and the depletion region. Thus, if the thickness of the resistive sea is 1/6 of the depletion width, then

$$\Delta V_2/\Delta V_1 = 6/7.$$

The significance of this voltage ratio is that the scanning beam cannot re-establish the full value of reverse bias across the diode in one sweep even with arbitrarily large beam currents. While the charge stored on the oxide surrounding the diode has been neglected in this discussion, a similar conclusion would result from a calculation which included this additional charge.

One important question about the resistive sea structure that has not yet been answered is whether a film resistivity can be chosen which will lead to an increase in the effective beam landing area of each p-type region without significantly affecting the resolution capabilities of the basic diode array. Answering this question requires an evaluation of the amount of charge stored on the resistive film over the oxide surrounding the diode relative to the amount of charge stored on the diode. This evaluation in turn requires a complicated model which includes the effects of the isolated p-regions and is beyond the scope of this paper. However, preliminary calculations indicate that there is a value of R_f which will preserve the resolution capabilities of the diode array and will also lead to a significant increase in the beam landing area of each p-type island. The optimum value of R_f is a strong function of the target geometry but will always be in the range of 10^{12} to 10^{14} ohms per square for practical geometries.

VI. MISCELLANEOUS TOPICS

The dark current characteristics of a diode array target are predominantly determined by the surface states at the silicon-silicon dioxide interface, as discussed by Buck and others.[13] However the detailed behavior of the dark current versus target voltage depends upon many other factors some of which are discussed in this section.

6.1 *Effect of Resistivity Striations on Dark Current*

A large number of the silicon diode array camera tubes fabricated to date have exhibited a phenomenon called "coring." Coring manifests itself as a modulation of the dark current pattern as illustrated in Fig. 24. The photographs in the figure are of the video display of the dark current pattern of a diode array camera tube at different target

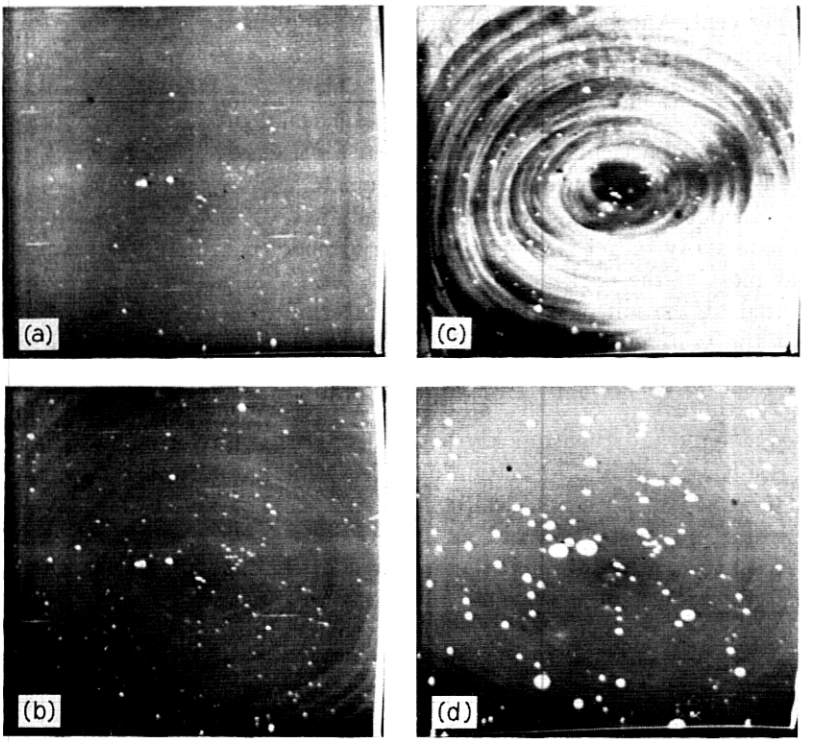

Fig. 24 — Photographs of the video display of the dark current pattern of a camera tube which exhibits "coring": (a) $V_T = 4$ volts, (b) $V_T = 6$ volts, (c) $V_T = 8$ volts, (d) $V_T = 12$ volts.

voltages. The modulation introduced by the coring pattern is seen to be a strong function of the target voltage; its maximum amplitude can be as high as 40 per cent. The spatial wavelength of the coring pattern is typically of order 500μ. The term modulation as used here means the ratio of the peak-to-peak modulation of the dark current, introduced by the coring, to the average dark current.

One possible cause of the coring, consistent with experimental results, is resistivity striations produced in the silicon substrate during crystal growth. The standard methods used for growing silicon crystals would result in circular striations.[20] In addition, a silicon crystal in which resistivity striations had been purposely introduced yielded targets which exhibited coring patterns that corresponded to the resistivity striations. A variation in resistivity of approximately 25 per cent yielded coring patterns with a modulation of approximately

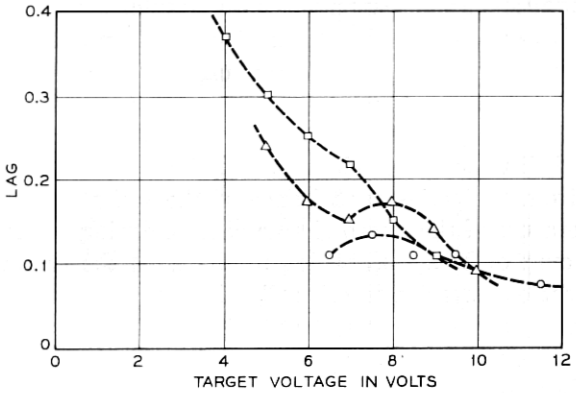

Fig. 29 — Image lag as a function of target voltage for different video signal levels: □ = 50 nanoamps, △ = 200 nanoamps, ○ = 500 nanoamps.

VII. CONCLUSION

The preliminary results reported in this paper indicate the silicon diode array camera tube has improved lag and spectral response and comparable resolution capabilities when compared with commercially available vidicons. In addition, the unity gamma of a diode array camera would be a significant advantage for color television cameras.

Two of the outstanding features of the silicon diode array camera are its wide spctral response (0.4 to 1.0μ) and its high effective quantum yield (approximately 50 percent). For fluorescent illumination these provide a sensitivity of approximately 1.3 μamp per ft-cd of faceplate illumination with an image sensing area of 1.8 sq-cm.

The expected operating life of a silicon diode array camera should exceed that a vidicon for at least two reasons. First, the image sensing target is not damaged by intense light images (for example, the noonday sun has been imaged with a F:1.5 lens on the silicon target without damage) Second, the completely assembled tube can be vacuum baked at 400°C provided an appropriate resistive film is used. This vacuum bake should provide a longer cathode life.

Typical video performance of a diode array tube is illustrated by Figs. 30, 31, and 32. These photographs were obtained from a 525-line monitor when the image of a black and white transparency was focused onto the camera. The photograph in Fig. 32 was obtained by reducing the size of the raster on the diode array so that only a small portion of the array was scanned. This electronic zooming permits

the individual diodes to be observed for detailed study. For example, the one very bright spot or white defect on the number 300 results from a single defective diode. The two bright spots on the extreme left represent two defective diodes separated by a good diode. For this photograph the optical magnification was adjusted so that the black and white wedge pattern created 300 cycles per inch at the center of the display. Since the diodes are located on 20μ centers, only two diodes are fully illuminated by a white bar near the numeral 300.

While the bright defects depicted in the photographs of Figs. 30 to 32 impair the image quality and would in some instances prevent this tube from being used, the small size and number of defects would be

Fig. 30 — A video display obtained with a typical silicon diode array camera tube. The subject was a black and white transparency.

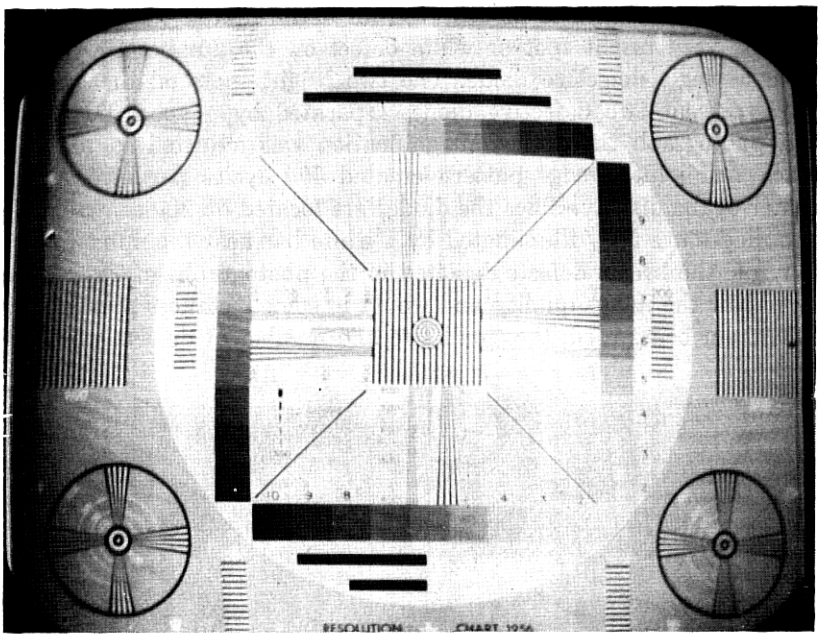

Fig. 31 — Video display of a resolution chart obtained with a silicon diode array camera tube.

acceptable in a number of applications. Although most of the arrays fabricated to date have exhibited bright defects, considerable progress has been made in reducing their number; improved technology should permit fabrication of defect-free arrays with moderately good yield.

VIII. ACKNOWLEDGMENTS

Although it is impossible to recognize individually all those who contributed to the work reported in this paper, we gratefully acknowledge the effective cooperation provided by everyone associated with the diode array camera tube program. The contributions of the people mentioned below were essential to the success of this program. Expert technical assistance was provided by P. M. Ryan and E. J. Zimany, Jr. The processing of the diode array targets was directed by T. M. Buck and J. V. Dalton; the mechanical design of the tubes was handled by E. J. Walsh, R. P. Hynes, and E. G. Olsen. Computational assistance was provided by A. J. Chick. Finally, the authors thank E. I. Gordon for the valuable stimulation he provided.

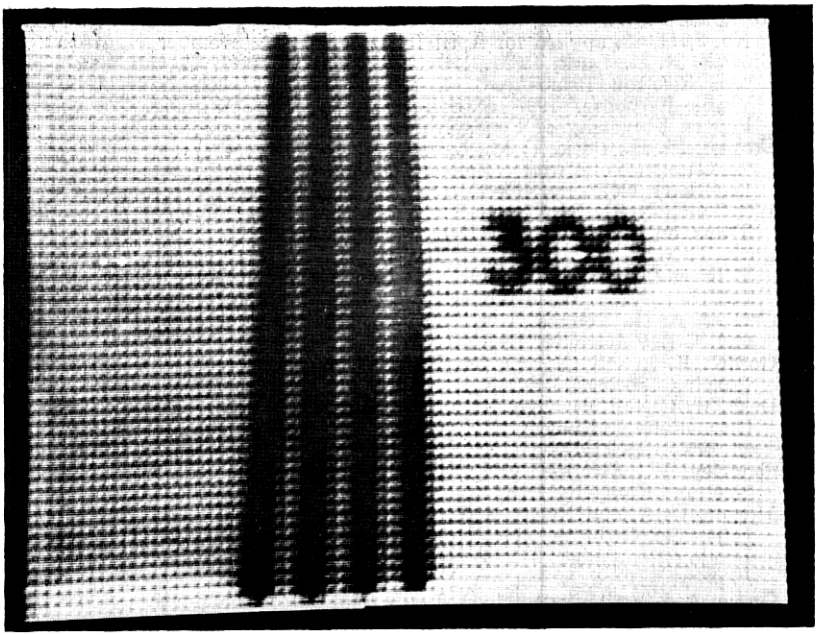

Fig. 32 — The video display of a small portion of the resolution chart shown in Fig. 30 obtained by electronically zooming the diode array camera. The white spots or defects correspond to diodes with a high value of reverse bias leakage current.

REFERENCES

1. Zworykin, V. K. and Morton, J. A., *Television,* New York: John Wiley and Sons, 2nd ed., 1954.
2. Weimer, P. K., Forgue, J. V., and Goodrich, R. R., "The Vidicon Photoconductive Camera Tube," RCA Rev., *12,* No. 1 (September 1951), pp. 306–313.
3. de Haan, E. F., van der Drift, A., and Schampers, P. P. M., "The 'Plumbicon,' a New Television Camera Tube," Philips Technical Rev., *25,* No. 6 and 7, (1963 and 64), pp. 133–155.
4. Horton, J. W., Mazza, R. V., and Dym, H., "The Scanistor—A Solid State Image Scanner," Proc. IEEE, *52,* No. 12 (December 1964), pp. 1513–1528.
5. Weimer, P. K., Sadasiy, G., Borkan, H., Meray-Horvath, L., Meyer, J., Jr., and Schallcross, F. V., "A Thin Film Solid-State Image Sensor," 1966 Int. Solid State Circuits Conf., University of Pennsylvania, Digest of Technical Papers, pp. 122–123.
6. Weckler, G. P., "Storage Mode Operation of Phototransistor and Its Adaption to Integrated Arrays for Image Detection," 1966 Int. Electron Device Meeting, Washington, D. C., October 26-28, 1966, p. 34.
7. Schuster M. A. and List, W. F., "Fabrication Considerations for Monolithic Electrooptical Mosaics," Trans. of the Metallurgical Soc. of AIME, *236,* No. 3 (March 1966), p. 375–378.
8. Papers in "Special Issue on Solid State Imaging," IEEE Trans. on Elec. Devices, *ED-15,* No. 4 (April 1968).

9. Reynolds, F. W., "Solid State Light Sensitive Storage Device," U. S. Patent No. 3,011,089, applied for April 15, 1958, issued November 21, 1961.
10. Crowell, M. H., Buck, T. M., Labuda, E. F., Dalton, J. V., and Walsh, E. J., "An Electron Beam-Accessed, Image-Sensing Silicon-Diode Array with Visible Response," 1967 Int. Solid State Circuits Conf., Digest of Technical Papers, University of Pennsylvania, March 1967, pp. 128–130.
11. Crowell, M. H., Buck, T. M., Labuda, E. F., Dalton, J. V., and Walsh, E. J., "A Camera Tube with a Silicon Diode Array Target," B.S.T.J., *46,* No. 2 (February 1967), pp. 491–495.
12. Wendland, P. H., "A Charge-Storage Diode Vidicon Camera Tube," IEEE Trans. on Elec. Devices, *ED-14,* No. 9 (June 1967), p. 285–291.
13. Buck, T. M., Casey, H. C., Jr., Dalton, J. V., and Yamin, M., "Influence of Bulk and Surface Properties on Image Sensing Silicon Diode Arrays," B.S.T.J., *47,* No. 9 (November 1968), pp. 1827–1854.
14. Chester, A. N., Loomis, T. C., Weiss, M. M., "Diode Array Camera Tubes and X-Ray Imaging," B.S.T.J., *48,* No. 2 (February 1969), pp. 345–381.
15. Gordon E. I. and Crowell, M. H., "A Charge Storage Target for Electron Imaging Sensing," B.S.T.J., *47,* No. 9 (November 1968), pp. 1855–1873.
16. Dash, W. C. and Newman, R., "Intrinsic Optical Absorption in Single-Crystal Germanium and Silicon at 77°K and 300°K," Phys. Rev., *99,* No. 4 (August 15, 1955), pp. 1151–1155.
17. Shockley, W., *Electrons and Holes in Semiconductors,* New York: D. van Nostrand Company, Inc., 1950.
18. Morton, G. A. and Ruedy, J. E., "The Low Light Level Performance of the Intensifier Orthicon," in *Photo-Electronic Image Devices,* symposium at London September 3–5, 1958, in *Advances in Electronics and Electron Physics,* XII, ed. L. Marton, New York: Academic Press, 1960, pp. 183–193.
19. Grove, A. S. and Fitzgerald, D. J., "Surface Effects on p-n Junctions: Characteristics of Surface Space-Charge Regions Under Non-Equilibrium Conditions," Solid State Elec., *9,* No. 8 (August 1966), p. 783–806.
20. Dikhoff, J. A. M., "Inhomogeneities in Doped Germanium and Silicon Crystals," Philips Technical Rev., *25,* No. 8 (1963 and 64), pp. 195–206.
21. Redington, R. W., "The Transient Response of Photoconductive Camera Tubes Employing Low Velocity Scanning," IRE Trans. on Elec. Devices, *ED-4,* No. 3 (July 1957), pp. 220–225.